RSC Advances

ROYAL SOCIETY OF CHEMISTRY

www.rsc.org/advances

Amine-Functionalized Multiwall Carbon Nanotubes Impart Osteoinductive and Bactericidal Properties in Poly(ε-caprolactone) Composites

Sachin Kumar, Suryasarathi Bose, Kaushik Chatterjee*

Department of Materials Engineering

Indian Institute of Science, Bangalore 560012 India

* *author to whom all correspondence should be addressed*

Email: kchatterjee@materials.iisc.ernet.in

Tel: +91-80-22933408

Abstract

Poly(ε-caprolactone) (PCL) is an aliphatic polyester widely used for biomedical applications but lacks the mechanical properties desired for many load-bearing orthopedic applications. The objective of this study was to prepare and characterize PCL composites incorporating multiwall carbon nanotubes (MWNTs) with different surface functional groups. PCL composites were prepared by melt-mixing with three different types of MWNTs: pristine (pMWNT), amine functionalized (aMWNT), and carboxyl functionalized (cMWNT). Melt rheology and scanning electron microscopy indicated good dispersion of the nanotubes in the matrix. Tensile strength and elastic modulus of the polymer was significantly increased by the incorporation of MWNTs and further enhanced by favorable interactions between PCL and aMWNTs. Thermal analysis revealed that MWNTs act as heterogeneous nucleation sites for crystallization of PCL and increase polymer crystallinity. Incorporation of functionalized MWNTs increased surface water wettability of PCL. Osteoblast proliferation and differentiation was significantly enhanced on functionalized composites. aMWNT composites also exhibited best bactericidal response. This study demonstrates that surface functionalization of MWNTs profoundly influences the properties of PCL and amine-functionalization offers the optimal combination of mechanical properties, osteogenesis and antimicrobial response. These results have important implications for designing nanocomposites for use in orthopedics.

Keywords: Polymer nanocomposites; Multiwall carbon nanotubes; Osteoblasts; Osteogenesis; Antimicrobial surface

1. Introduction

There are growing incidences of chronic, degenerative diseases globally largely driven by sedentary, stressful modern lifestyles and age-related injuries with increasing life spans [1]. As a result, there is an ever-increasing demand for therapies that can facilitate regeneration and replacement of damaged tissues [2]. Globally there is huge demand for bioactive materials for bone tissue engineering (BTE). Ideally, for BTE application a bone substitute material minimally should be biocompatible and osteoconductive to enhance new bone growth [3, 4]. In recent years, several types of bioactive materials such as bioactive glass, hydroxyapatite, β-tricalcium phosphate, glass ceramics, etc., have been used for BTE, but these materials tend to be brittle and many are non-biodegradable [5].

With progressive advancement in the field of tissue engineering, interest has shifted to the use of synthetic biodegradable polymers as scaffold materials [5]. These synthetic polymers are gaining attention because they can offer structural integrity and mechanical strength, and eventually slowly degrade leaving behind newly formed tissue which is expected to take over the mechanical loads [5]. Many synthetic biodegradable polymers have been used as scaffolds for tissue engineering, among which poly(ε-caprolactone) (PCL) has been extensively studied [6]. PCL is a semicrystalline, hydrophobic polymer with a slow degradation rate. PCL also exhibits excellent bioresorbability and biocompatibility. However, PCL lacks mechanical properties desired for use in load-bearing applications limiting its use in orthopaedics [6].

There are various routes available to improve the mechanical properties of a polymer but one the most effective ways is by reinforcing the soft matrix with hard nanoparticles [7-10]. Among the many possible nanofillers, multiwall carbon nanotube (MWNT) reinforcement has been shown to effectively strengthen polymers due to its good mechanical properties [7, 10, 11]. In a recent review various aspects of polymer/CNT composites have been addressed [12]. MWNT-polymer composites are being increasingly studied for potential use in biomedical

applications [13]. Zhang et al. showed that the addition of MWNTs in polylactic acid (PLA) improved mechanical properties but inhibited growth of fibroblast on the composite surface [14]. Pan et al. reported that bone marrow derived stem cell osteogenesis was enhanced in PCL scaffolds with the incorporation MWNTs [7]. Studies have also shown that the use of surface functionalized MWNTs, surfactant-coated MWNTs and MWNTs decorated with block co-polymers help in better dispersion and polymer-nanotube interfacial interactions. This results in more effective stress transfer to MWNTs resulting in improved mechanical properties of the composites [15-17]. Lin et al showed that carboxylated MWNTs were better dispersed than MWNTs in poly(lactic-co-glycolic acid) (PLGA) [18]. Better nanoparticle dispersion resulted in further improvement in mechanical properties of the polymer. Other studies have reported that functionalization of MWNTs leads to reduced cytotoxicity in contrast to non-functionalized and surfactant-coated nanotubes [19, 20].

However, the role, if any, of surface functional groups of MWNT fillers on the physical properties and biological response to biomedical polyesters has not been studied. Thus, the aim of this study was to systematically evaluate the effect of using functionalized MWNTs in PCL and compare with non-functionalized MWNT-reinforced PCL and neat polymer. We hypothesized that the presence of functional groups on the nanoparticles will lead to differences in physical properties and biological responses. PCL/MWNT composites containing 1% MWNTs were prepared by melt mixing and their thermal, rheological and mechanical properties were characterized to study the effect of MWNT functionalization. Osteoblast attachment, proliferation and mineralization along with bactericidal property were studied to characterize potential differences in biological response.

2. Materials and Methods

2.1. Materials

Chemical vapor deposition-synthesized, thin purified MWNTs: pristine (pMWNT), ~COOH functionalized (cMWNT) and ~NH_2 functionalized (aMWNT) were obtained commercially (Nanocyl CA). Table 1 presents average diameter, length, aspect ratio and percentage functionalization of the different MWNTs. pMWNTs were processed to enhance their dispersion by dissolving in dimethylformamide (DMF, Merck) followed by probe sonication (Hielsher, Ultrasound technology) and vacuum drying overnight at 80°C. cMWNTs and aMWNTs were used as received without further treatment. PCL (average molecular weight M_n = 45,000 g/mol, Sigma-Aldrich) obtained in pellet form was dried overnight in a vacuum oven at 30°C prior to preparing composites.

2.2. Preparation of PCL/MWNT nanocomposites

Nanocomposites of PCL/MWNT were prepared by melt mixing. 1 wt% (MWNT to PCL ratio) of the respective MWNTs was mixed with PCL using a conical twin screw microcompounder (Haake Mini lab II) at 80°C with rotating speed of 60 rpm under nitrogen supply for 20 min to form nanocomposites of PCL/pMWNT, PCL/cMWNT and PCL/aMWNT . Melt extruded strands were compress-molded using a laboratory scale hot press at a pressure of 30 kgf/m^2, melting temperature 80°C and holding time of 2 min into circular discs (5 mm diameter X 0.5 mm height).

2.3. Physical and chemical characterization

Surface morphology of neat PCL and its PCL/MWNT nanocomposites was analyzed using a scanning electron microscope (SEM). The extruded strands were cryo-fractured in liquid nitrogen. Cryo-fractured samples were mounted on an aluminium stub and sputter-coated with gold prior to imaging (FEI Sirion XL30 FEG).

Thermal properties were characterized by differential scanning calorimetry (DSC, Mettler-Toledo DSC). The samples were heated from 25°C to 100°C, held for 3 min, cooled to 25°C, and reheated to 100°C to eliminate prior thermal history, at 10°C/min under argon atmosphere. The degree of crystallization (X_c) of samples were calculated as follows: $X_c = (\Delta H_c / \Delta H_0)^* 100$, where ΔH_c is the heat of crystallization of the sample and ΔH_0 is heat of fusion of a fully crystalline material (ΔH_0 for PCL was taken as 139.5 J/g) [21]. X-ray diffraction (XPERTPro, PANalytical) patterns were recorded at ambient temperature using a Cu Kα radiation source (40kV and 20mA) in the 2θ range of 10° to 40°.

The viscoelastic properties of neat PCL and its nanocomposite were measured by a stress controlled rheometer (Discovery Hybrid Rheometer, DHR-3, TA Instruments) using parallel plate geometry (25 mm diameter). The samples of 1 mm thickness were melted at 70°C for 5 min in the fixture to remove residual thermal history, and subsequently small amplitude oscillatory shear (SAOS) were carried out. The dynamic strain sweep measurements were carried out *apriori* to ensure that the strain amplitude was within the linear viscoelastic region. Isothermal dynamic frequency sweep measurements were performed on all samples from 0.01 rad/sec to 100 rad/sec at 70°C under inert N_2 atmosphere to prevent thermal degradation.

Uniaxial tensile tests was performed in accordance with ASTM standard D368 type V. Tensile tests (MicroUTM-Mecmesin) were performed at room temperature using 100 N load cell at a cross head speed of 5 mm/min. Data are presented as mean ± S.D. from five independent measurements. The elastic modulus of the sample was calculated using the initial linear part of the stress–strain curve and tensile strength was taken as the stress at which facture occurred.

Sessile drop water contact angle goniometry (OCA 15EC, Dataphysics) was used to assess surface wettability. Ultrapure water (Sartorius Arium) was used as the probe liquid. The contact angles reported represent the mean for three independent measurements.

Surface topography of neat PCL and its nanocomposite discs used for cell studies were measured using an atomic force micoscope (AFM, Bruker Dimension Icon) in tapping mode at resonance frequency of about 300 kHz - 410 kHz. Surface information was expressed as height images from 1.5 X 1.5 μm^2 AFM scan.

2.4. Biological studies

MC3T3-E1 subclone 4 mouse osteoblasts (ATCC, USA) were cultured in alpha-minimum essential medium (α-MEM, Gibco, Life Technologies) with 10% (v/v) fetal bovine serum (FBS, Gibco, Life Technologies) and 1% (v/v) penicillin- streptomycin (Sigma) in 5% CO_2 atmosphere at 37 °C. Medium was changed every 3 d until cells were 80% to 90% confluent. The cells were passaged using 0.25% trypsin (Gibco) and serially subcultured. Passage 3 cells were used for all studies reported here.

Compression molded discs (5 mm diameter X 0.5 mm height) were placed in 96 well polypropylene plates (Sigma, non-surface treated) to minimize cell attachment to the bottom of the wells. The well-plates containing the discs were sterilized using ethylene oxide (Anprolene gas sterilizer, Andersen) and degassed for 4 d under vacuum prior to cell seeding. 0.2 mL medium containing 5 X 10^3 cells were added to each well and cultured as described above with media changes every 3 d. Three plates were used for this study for measuring cell response at 1 d, 6 d, and 10 d after seeding. Each plate contained at least five samples each of PCL, PCL/pMWNT, PCL/aMWNT, and PCL/cMWNT wherein at least three samples were used for DNA quantification and two samples were used for nuclear staining. This experiment was repeated thrice independently.

Picogreen dsDNA quantification kit (Invitrogen) was used to quantify DNA content on the sample [22, 23]. To collect the DNA, 0.2 mL lysate solution (0.2 mg/ml proteinase K and 0.02% sodium dodecyl sulfate) was added for 24 h at 37°C. 0.1 mL of the lysate was transferred to a fresh 96 well-plate and mixed with equal volume of the picogreen dye solution. Fluorescence intensity was measured using 485 nm excitation and 520 nm emission in a fluorescence spectrophotometer (Synergy HT, BioTek). DNA content was calculated from a standard plot generated by serial dilutions of a DNA solution of known concentration. A total of fourteen samples ($n \geq 3$ for three independent experiments) were used to measure DNA content for each composite.

Cells were fixed with 3.7% (mass/volume) formaldehyde in PBS for 15 min, permeabilized with 0.2% TritonX-100 for 5 min and stained with 6.6 μM Alexa Fluro 546 (Invitrogen) for 1 h and 14.3 mM DAPI for 15 min for actin filaments and nuclei, respectively. Stained cells were imaged in the blue and red channel using an inverted fluorescence microscope (Olympus IX-71). ImageJ software was used to calculate cell area and aspect ratio. An outline of the cell was created to measure its area and an ellipse was fitted to calculate aspect ratio.

To study mineralization, MC3T3 cells (5×10^3/well) were added in a 96 well plate containing nanocomposites discs as above and incubated in growth media for 1 d. Growth media was replaced with osteogenic differentiation media (growth media supplemented with 50 μg/ml ascorbic acid and 10 mM β -glycerophosphate [24]). Medium was refreshed every 3 d. Cells were fixed with 3.7% formaldehyde solution at 14 d and 21 d. Calcium deposition was analysed by staining with 2% Alizarin Red S (ARS) (Sigma). Fourier transform infrared (FTIR) spectroscopy was measured from 650 cm^{-1} to 4000 cm^{-1} to analyse the presence of calcium phosphate. For quantification, the stain was desorbed with 0.5 ml of 5% SDS in 0.5

N HCL for 30 min at room temperature [25]. 150 µl of solubilised stain was collected in a 96 well plate, and absorbance was measured at 405 nm using a spectrophotometer.

2.5 Antibacterial test

E.coli (MG 1655) were cultured in sterile Luria Broth (LB) media overnight at 200 rpm and 37 °C. The *E.coli* was harvested by centrifugation at 3000 rpm for 10 min. The collected pellet was suspended in phosphate buffer saline (PBS) and the optical density (OD) of the suspension was adjusted to 0.5 at 600 nm. This suspension culture was used as inoculums for further work.

The direct contact test was used to assess the antibacterial properties of PCL and the composites. 50 µl of the bacterial suspension was added to a 96 well polystyrene plate with sterilized discs as described above for osteoblast studies. Empty wells without discs were used as controls. 200 µl of LB media was added to each well and incubated at 37 °C with constant shaking at 50 rpm. The growth of suspended bacteria in contact with the different surfaces was evaluated at 0 h, 1 h, 3 h, 5 h, 8 h, 12 h, 18 h and 24 h by collecting 200 µl of the suspension and measuring the OD at 600 nm using a spectrophotometer. All measurements are reported as mean ± S.D. for $n \geq 3$. To image adherent cells, samples were fixed with 2.5% glutaraldehyde for 1 h, dried and sputter-coated with gold prior to SEM imaging.

2.6. Statistical analysis

For statistical analyses, 1-way ANOVA (analysis of variance) with Tukey's test for multiple comparisons was used. Differences were considered statistically significant if $p < 0.05$ and are indicated by symbols in the figures.

3. Results

3.1. State of MWNT dispersion

SEM micrographs (Fig. 1) of cryo-fractured surfaces of neat PCL and the different PCL/MWNT nanocomposites show the state of dispersion MWNTs in the PCL matrix. MWNTs are seen as white specks indicated by the arrows. Higher magnification images are presented as insets in figures 1(b)-1(d). Figs 1(b) to 1(d) show uniform dispersion of the different types of MWNTs in PCL.

3.2. Thermal and XRD analyses

DSC was used to analyze melting and crystallization behavior of neat PCL and its different nanocomposites. Melting endotherm for PCL shown in Fig. 2(a) indicates that the melting temperature (T_m) of neat PCL is 55.4 °C and those of the composites lie in the range of 56°C to 58°C. Fig. 2(b) presents the crystallization exotherms for neat PCL and the PCL/MWNT composites. Table 2 compiles the thermal properties of PCL, PCL/pMWNT, PCL/cMWNT and PCL/aMWNT nanocomposites. Crystallization temperature (T_c) and the degree of crystallization (X_c) of PCL increased with addition of MWNTs. All the nanocomposites showed T_c of approximately 42°C. However, differences in the heat of crystallization (ΔH_c) are evident from changes in the width of the crystallization peaks. XRD patterns (Fig. 3) indicate the presence of two strong diffraction peak at Bragg angle 2θ = 21.2° and 23.5°. These peak positions remain unchanged in the composites. However, the intensity of the peaks increased in the composites compared to neat PCL.

3.3. Rheology

Rheological properties of the nanocomposites were measured in the linear viscoelastic regime limited to a narrow strain region. The storage modulus (G') and complex viscosity

(η^*) obtained from the dynamic frequency sweep measurements for neat PCL and the nanocomposites are shown in Figs. 4(a) and 4(b), respectively. The dependence of G' on ω attenuates at lower frequencies on addition of MWNTs to PCL. This leads to restrained large-scale polymer relaxations in the presence of MWNTs. In addition, frequency-independent plateaus for G' for $\omega < 1$ rad/s in the presence of 1 wt % pristine and amine-functionalized MWNTs suggest that rheological percolation was achieved (Fig. 4(a)).

3.4. Tensile test

The stress-strain curves for neat PCL and PCL/MWNTs composites are presented in Fig. 5(a). Figs. 5(b) and 5(c) compile elastic modulus and tensile strength, respectively, for the different samples calculated from stress-strain plots. Addition of MWNTs in PCL significantly increased both elastic modulus and tensile strength of PCL. The elastic modulus of PCL increased by 30% from 337 MPa ± 8 MPa to 439 MPa ± 13 MPa on addition of pMWNTs. Equivalent addition of cMWNTs and aMWNTs led to 13% (382 MPa ± 7 MPa) and 29% (435 MPa ± 12 MPa) increase in moduli, respectively. Similarly, the tensile strength of neat PCL (15.2 MPa ± 0.8 MPa) increased significantly by 21% (18.5 MPa ± 0.8 MPa), 14% (17.3 ± 1.3 MPa) and 28%, (19.4 ± 0.9 MPa) for composites of pMWNTs, cMWNTs, and aMWNTs, respectively. Stress-strain curve also shows that addition of MWNTs in PCL matrix led to decrease in elongation as composites became more brittle (Fig.5(a)).

3.5. Surface wettability and roughness

Static water contact angle on surface of PCL and its nanocomposites are compiled in Fig. 6. Incorporation of functionalized MWNTs in PCL led to a decrease in contact angle. Contact angle of PCL increased significantly from 78.9° ± 0.3° to 84.1° ± 2.8° with reinforcement with pMWNTs. There was a significant decrease in water contact angle to 71.9° ± 0.6° and 73.8° ± 0.4° with addition of cMWNT and aMWNT, respectively. Surface

topographies of neat PCL and its nanocomposite discs used for cell studies characterized by AFM are presented in Fig. 7. AFM results shows that arithmetic roughness (R_a) was 1.9 nm for PCL, and increased to 4.5 nm, 3.9 nm, and 3.1 nm for PCL/pMWNT, PCL/cMWNT and PCL/aMWNT discs, respectively.

3.6. Osteoblast response

To evaluate these composites for potential use in orthopedics, osteoblast response to the composites was systematically studied in vitro and compared with neat PCL. Cell attachment (1 d) and proliferation (6 d and 10 d) were quantified by assaying the DNA content and qualitatively assessed by imaging fluorescently-stained nuclei. DNA content was taken as a measure of cell numbers. Fig. 8 shows DNA content on PCL, PCL/pMWNT, PCL/cMWNT and PCL/aMWNT discs at 1 d, 6 d and 10 d of MC3T3-E1 cell culture. DNA content at 1 d was marginally but statistically-significantly higher on PCL than the three composites suggesting that fewer cells attached to the composites than on neat PCL. The DNA content increased on all samples from 1 d to 6 d and then further at 10 d. Note that the DNA content approximately doubled from 1 d to 6 d but there was smaller increase (approximately 15% to 20%) from 6 d to 10 d. Statistical analyses ($p < 0.05$) indicate that the DNA contents at both 6 d and 10 d on PCL/cMWNT and PCL/aMWNT were similar and significantly higher (approximately 10% to 15%) than on PCL/pMWNT and PCL, both of which were statistically similar.

Fig. 9 presents fluorescence micrographs of MC3T3-E1 cell nuclei cultured on PCL, PCL/pMWNT, PCL/cMWNT and PCL/aMWNT discs at 1 d, 6 d and 10 d. After 1 d culture few nuclei were seen on all the substrates. The number of nuclei increased on all samples from 1 d to 6 d and then further at 10 d indicating that the osteoblasts were proliferating on all surfaces. These results corroborate the findings of the DNA assay. There was little

discernable difference between the different samples at a given day possibly due to the relatively small differences as quantified by the DNA assay. In contrast, the changes between 1 d to 6 d or 10 d were more significant both visually and as revealed the DNA assay.

Fluorescence micrographs were used to characterize morphology of the osteoblasts on PCL and PCL/MWNT composites at 1 d (Fig. 10). Quantitative evaluation of spread area and aspect ratio revealed statistically significant differences in osteoblast morphology on PCL was higher compared to the nanocomposites. Cells assumed a rounded (aspect ratio of 1.0 to 1.5) and well spread (large surface area) morphology on PCL surfaces. The cells were rounded but less well spread (smaller surface area) on PCL/pMWNT. The cells were significantly more elongated (aspect ratio of 2.5 to 3.5) and less spread (smaller surface area) on PCL/aMWNT and PCL/cMWNT surfaces.

The chemical nature of the mineral deposited by the differentiating osteoblasts was confirmed by FTIR. Characteristic phosphate group peaks at 995 cm^{-1} and 1077 cm^{-1} and the shoulder at 1015 cm^{-1} seen on PCL/aMWNT disks at 21d Fig. 11(a) indicate calcium phosphate deposition [26]. Quantification of ARS staining revealed higher calcium deposition on functionalized MWNTs composites discs (Fig. 11). Mineralization increased from 14 d to 21 d on all surfaces (Fig. 11). The eluent collected from PCL/aMWNT composite showed significantly higher absorbance than the cMWNT composite which was significantly higher than from other surfaces indicating largest calcium deposition on PCL/aMWNT composites.

3.7. Antibacterial Test

E.coli were used to investigate potential bactericidal property of neat PCL and the different PCL/MWNT composites discs by direct contact test [27]. Fig. 12 shows changes in OD for *E.coli* growth with time. OD of bacterial culture increased linearly up to 3 h on neat PCL and all three nanocomposites with no significant differences. However after 5 h

PCL/aMWNT, PCL/cMWNT, PCL/pMWNT composites showed lower OD compared to neat PCL and the blank control (Fig. 12). Functionalized MWNT composites showed better antibacterial properties that neat PCL and PCL/pMWNT. PCL/aMWNT composite showed least OD compared to PCL, PCL/pMWNT and PCL/cMWNT. Fig. 13 (a-d) shows SEM micrographs of bacterial cells adhered to PCL and its nanocomposites at 8 h. SEM images of bacteria covering the nanocomposites surface showed rough surface morphology compared to those on PCL. Cells on PCL/cMWNT and PCL/aMWNT composites showed irreversible membrane damage as shown in Fig. 13 insert.

4. Discussion

PCL is a polyester widely used for biomedical applications but lacks the mechanical properties desired for orthopedic use. The specific objective of this study was to prepare and characterize PCL/MWNT- composites for orthopedic applications. We hypothesized that the presence of functional groups on MWNTs could lead to interactions with the polymer backbone thereby leading to differences in composite properties as well biological response. In this study, the nanofiller content was fixed 1 wt% for the three different types of MWNTs (pMWNT, aMWNTs, and cMWNT) because previous studies have shown that this fraction can improve mechanical properties [7, 28] without inducing significant cytotoxicity [29]. In this study, melt mixing was used to prepare the composites as it offers a solvent free, green route for fabrication [30]. Moreover, melt mixing affords faster processing than solution based techniques and is thus popular industrially for preparation of polymer blends and nanocomposites.

Effective dispersion of MWNTs in a polymer matrix depends on the prevention of formation of agglomerated bundles of individual nanoparticles [31]. Increased dispersion can be achieved either by sonication techniques to break agglomerated MWNTs or by surface

functionalization of MWNTs which may facilitate dispersion and interactions of MWNTs in polymer matrix [32, 33]. During melt mixing it is critical to maintain stable uniform dispersion of MWNTs and this can be achieved by optimizing operating parameters for processing of the PCL/MWNT composite [34]. SEM micrographs in Fig. 1 show that all the MWNTs were well dispersed in PCL matrix with no observable aggregates. This may be attributed to the following: (i) sonication of pMWNT prior to melt mixing helped in breaking agglomerated pMWNTs, (ii) surface functionalization of aMWNTs and cMWNTs resulted in good dispersion and compatibility with PCL, and (iii) optimal choice of operating parameters for melt mixing minimized secondary agglomeration during processing.

Thermal analysis revealed that the addition of MWNTs in PCL matrix did not affect T_m significantly indicating that the reinforcement of PCL matrix by MWNTs did not change the crystal structure of PCL [35-37] (Fig. 2). This was corroborated by XRD analysis (Fig. 3). Two strong diffraction peaks at $2\theta = 21.2°$ and 23.5° were observed for PCL corresponding to the (110) and the (200) lattice planes of orthorhombic crystalline form [38]. These peaks were also observed for the composites. The crystallization exotherms revealed that the addition of MWNTs in PCL matrix caused an in increase in T_c. It is likely that the MWNTs act as nucleating agents for crystallization of PCL [39, 40]. Nucleating action of MWNTs in a polymer matrix depends on the interaction between the polymer and MWNT surfaces [41]. Interactions between surface functional groups of MWNTs with PCL chains will cause the nanofiller to act as a more effective nucleating agent, thereby, shifting T_c to a higher temperature [37]. Comparison of thermal properties for the different samples (Table 2) shows that % crystallinity increased for all the nanocomposites. This indicates that well-dispersed MWNTs not only induced heteronucleation but also act as effective site for PCL to nucleate [42]. Interestingly, XRD patterns of the nanocomposites (Fig. 3) displayed the same diffraction

peaks as PCL but with higher intensity suggesting that the nanocomposites have higher crystallinity in comparison to neat PCL [43]. Thus, XRD data corroborates the DSC results.

Melt rheology of these composites (Figs. 4(a) and 4(b)) revealed that rheological percolation was achieved in PCL/pMWNT and PCL/aMWNT composites. From the complex viscosity behaviour it can be seen that MWNTs led to strong yield stress especially at lower frequencies indicating physical gelation [44]. Attaining rheological percolations with reinforcement of MWNTs in PCL matrix can be attributed to uniform dispersion of MWNTs in PCL matrix shown by SEM images (Fig. 1). A plausible explanation of this could also be the higher aspect ratio of pMWNT [40] which results in the restriction of movement of PCL chains. Thus, PCL/pMWNT composite showed high storage modulus than neat PCL (Fig. 4(a)). cMWNTs with lower aspect ratio (Table 1) exhibited lower modulus. In contrast, PCL/aMWNT showed rheological properties similar to those of PCL/pMWNT composites although the aspect ratio aMWNTs was the lowest among all the three MWNTs used. This is indicative of the presence of strong interfacial interactions between PCL and aMWNTs in the melt putatively between the amine groups of aMWNTs and the ester groups of the polymer chains. These findings can also be corroborated from the low frequency complex viscosity (η^*) plot (Fig. 4(b)). On addition of pMWNTs and aMWNTs, η^* considerably increased at low frequencies. Moreover, the Newtonian plateau of viscosity plots disappeared, suggesting strong shear thinning behaviour [44]. This indicates the formation of percolation network, also evident from frequency sweep for G'.

Tensile tests revealed that incorporation of MWNTs in PCL significantly improved elastic modulus and strength of all of the composites (Figs. 5(b) and 5(c)). However, pMWNTs and aMWNTs were most efficient in improving the mechanical properties of PCL. Improvement in mechanical property of nanocomposites depends primarily on the dispersion of the nanoparticle, its aspect ratio and strong filler-matrix interactions [31, 45]. Increase in the

elastic modulus and tensile strength of PCL with addition of MWNTs are attributed to (i) uniform dispersion of stiffer MWNTs in PCL matrix [28] as shown by SEM images of PCL/MWNT (Figs. 1(b) – 1(d)), and (ii) increase in crystallinity of PCL with addition of MWNTs as shown by DSC (Table 2), thereby strengthening the mechanical property of the matrix [46].

Enhancement in mechanical strength by mechanism of stress transfer between MWNTs and PCL is influenced by effective interaction between filler and matrix, and the length of nanotube [47-49]. Such interactions were evidenced by rheological percolation for PCL/pMWNT composite having longer pMWNT in PCL matrix (Fig. 4(a)), and favourable interaction between aMWNTs and PCL. Filler particles with a larger aspect ratio are believed to be better suited for effective load transfer in polymer composites [50]. In order to maximize mechanical properties of a composite, long nanotubes with higher aspect ratio are desired because composites mechanical properties directly depend on total surface area, which in turn depends on aspect ratio [45]. As a result, PCL/pMWNT composites incorporating longer pMWNTs (higher aspect ratio, Table.1) showed higher modulus and strength. Interestingly, PCL/aMWNT showed mechanical properties similar to those of PCL/pMWNT composites although aMWNTs had shorter length and lowest aspect ratio among all the three MWNTs due to the presence of strong interfacial interactions between PCL and aMWNT as observed in rheology (Fig. 4). A lower elastic modulus and tensile strength of PCL/cMWNT compared to PCL/pMWNT and PCL/aMWNT nanocomposites is due to the lack of strong interfacial interactions between the hydrophilic cMWNTs and the hydrophobic PCL matrix [46]. Taken together, uniform dispersion and favourable interaction of aMWNTs with PCL resulted in effective improvement in mechanical property PCL/aMWNT composite.

Water-wettability of its surface is believed to play a critical role in determining biological response to a material. Hydrophobicity of PCL is one of the major limitations of its

use as a tissue scaffold. Incorporation of MWNTs to PCL can influence water-wettability through potential changes in surface roughness and through the availability of functional groups on the surface. Surface functionalization of MWNTs results in increase in the surface energy of MWNTs due to the presence of the polar groups on MWNT surface [51]. Presence of polar components on functionalized MWNTs induces dipole-dipole and dipole-induced dipole interactions [31]. This may lead to increased wettability or a decrease in water contact angle with addition of functionalized MWNTs to PCL matrix. Thus, water contact angles on PCL/aMWNT and PCL/cMWNT were found to be lower than PCL or PCL/pMWNT (Fig. 6).

The interactions of cells to designed scaffolds are sensitive to surface topography [52, 53]. AFM analysis revealed that PCL/MWNT nanocomposites had higher surface roughness compared to neat PCL (Fig. 7). Change in surface roughness can be attributed to uniform dispersion of MWNTs in polymer matrix and their specific interaction with polymer [28]. Increase in polymer crystallinity can also result in increase of surface roughness [53]. As a result, all nanocomposite surfaces were rougher than PCL due to good dispersion of MWNTs in PCL matrix (Fig.1) and the resultant increase in crystallinity (Table 2). Results also indicate that the increase in surface roughness scaled with the length of MWNTs (Table 1). pMWNTs being the longest resulted in the largest roughness in the PCL composites followed by cMWNT and aMWNT nanocomposites.

Biomaterial surface properties play a key role in cell attachment, proliferation, morphology and differentiation by modulating intracellular signalling events [54-57]. In this study, osteoblast attachment and proliferation to the different substrates were compared (Figs. 8 and 9). Cells attached and proliferated on all the four substrates. Although cell attachment to the composites was marginally lower in contrast to the neat polymer, significantly more osteoblasts were observed at 6 d and 10 d on the functionalized-MWNT composites due to differences in cell proliferation. Thus, the addition of functionalized MWNTs to PCL resulted

in enhanced cytocompatibility of the polymer [7, 58]. Cell response to material substrates are influenced by many properties including its chemical properties and physical cues from the surface to the cells. The presence of MWNTs and their functionalization lead to differences in surface chemistry, nanoscale roughness, etc. potentially inducing changes in protein adsorption [59]. Here increased aspect ratio and cell proliferation on the functionalized-MWNT composites may be attributed to increased surface water wettability (Fig. 6) and surface roughness (Fig. 7). Wettability and rough surface profoundly influence protein adsorption to the surface [60, 61], an important event in the biological response to materials. Osteoblasts have been observed to attach more to hydrophilic surfaces than to hydrophobic surfaces [61]. Differences in surface topography are also known to influence cellular response by changes in focal adhesions and cell signalling pathways involved in mechanotransduction [62]. These differences are often associated with changes in cell morphology. Cell morphology has been predictably used an early marker of cell fate [63, 64]. In this, cells were assumed an elongated morphology on functionalized MWNT composites in contrast to the more rounded morphology on PCL and PCL/pMWNT surfaces (Fig. 10). In a recent study it was reported that human bone marrow mesenchymal stem cell osteogenesis was associated with an elongated, highly-branched morphology in contrast to the rounded morphology of cells that proliferate but did not differentiate [65]. A similar trend is observed here for elongated osteoblasts on functionalized MWNT composites that differentiated more in contrast to the rounded cells on PCL and PCL/pMWNT. Quantitative analysis of calcium deposition by the osteoblasts (Fig. 11) revealed highest osteogenesis on PCL/aMWNT compared to on neat PCL and the other composites. It has been reported that functional groups on a surface modulate the conformation of adsorbed protein which affects osteogenesis through changes in integrin binding independent of cell proliferation [66]. Amine and hydroxyl groups on the biomaterial surface were found to enhance osteogenic differentiation in contrast to surfaces

presenting carboxyl and methyl groups [66]. These findings reported previously are corroborated by the resulted presented herein. Taken together, results of this study elucidate the role of amine group on MWNT fillers in increasing the osteoconductivity of PCL.

Bacterial infections continue to be a major clinical challenge associated with the use of biomedical implants and a cause for device failures leading to morbidity and mortality aside from increased health care costs. Whereas increased osteoblast activity on surfaces of the functionalized MWNT composites is desired, it is desirable to minimze bacterial attachment and growth. Direct contact test indicated that functionalized MWNT composites impart bactericidal property to PCL surfaces (Figs. 12 and 13). The enhanced bactericidal nature of the MWNT composites can be attributed due to synergetic effect caused by physical and chemical interaction between polymer and nanoparticles [67]. Studies have shown that bactericidal property of nanoparticles is related to cell membrane disruption by oxidative stress [68-71]. Another mechanism by which carbon nanotubes show bactericidal property is through cell membrane disruption on direct contact with bacteria [67, 72, 73] (Fig. 13). The highest bacterial resistance of PCL/aMWNT was associated with extensive cell membrane lysis on the composite surface. It is well reported that quaternary ammonium imparts bacterial resistance to a surface by disrupting the bacterial membrane leading to cell lysis [74]. Although less effective than quaternary ammonium, primary amine groups are also reported to be effective in reducing cell increasing bacterial resistance [75]. Thus, it appears that the presence of amine groups on MWNT fillers can also increase the bacterial resistance of PCL.

Table 3 summarizes the key outcomes of this work on the use of functionalized MWNTs as fillers in PCL matrix for orthopedic applications. Physical characterization suggests that the incorporation of 1 wt% MWNTs enhances mechanical properties of PCL with the highest improvements observed with the use of pMWNTs and aMWNTs. Biological studies indicate that PCL/aMWNT and PCL/cMWNT composites were better substrates for

proliferation and differentiation of osteoblasts than PCL and PCL/pMWNT. Antibacterial property studies indicate that PCL/aMWNT and PCL/cMWNT composites showed better bacterial resistance than PCL and PCL/pMWNT. Thus, surface functionalization of MWNTs is critical for preparation of PCL nanocomposites for orthopedic applications and PCL/aMWNT composites were optimal in terms of both superior mechanical properties and biological outcomes.

5. Conclusions

This study highlights the critical role of surface functionalization of nanofillers in biomedical polymers. The incorporation of MWNTs in PCL improved mechanical properties of the composites and was enhanced by the presence favorable interactions between aMWNTs and the PCL matrix. Cell studies indicate that aMWNTs increased osteogenesis. Bacterial studies revealed that aMWNT was most effective in improving the bactericidal property of PCL. Taken together, amine functionalization of MWNTs yielded PCL composites with optimal combination of improved mechanical properties and desired biological response.

Acknowledgements

This work was funded by the Department of Atomic Energy- Board of Research in Nuclear Sciences, India (DAE/BRNS). K.C. was supported by the Ramanujan fellowship from the Department of Science and Technology (DST), India. Authors gratefully acknowledge technical assistance from Ms. Priti Xavier with rheology, Mr. Shyam Sundar for contact angle measurements, Mr. Prasanna Kumar S. Mural for tensile test and Mr. Mohan Chokkalingam for his technical assistance with antimicrobial test.

List of Tables:

Table 1: Average diameter, length and percentage functionalization of the MWNTs (as provided by the supplier)

MWNT	Code No.	Average Diameter (nm) (d)	Average Length (μm) (L)	Aspect Ratio (L/d)
Pristine (pMWNT)	NC-7000	9.5	1.5	158
~COOH functionalized (cMWNT)	NC-3151	9.5	1.0	105
~NH_2 functionalized (aMWNT)	NC-3152	9.5	0.7	73

Table 2: Thermal properties of PCL, PCL/pMWNT, PCL/cMWNT and PCL/aMWNT nanocomposites determined from DSC analysis

Sample	T_m (°C)	ΔH_m (J/g)	T_c (°C)	ΔH_c (J/g)	X_c (%)
PCL	55.4	51.9	32.4	49.9	35.8
PCL/pMWNT	57.1	53.9	42.3	53.7	38.5
PCL/cMWNT	56.7	52.1	40.1	52.6	37.7
PCL/aMWNT	57.3	54.8	42.4	57.1	40.9

Table 3: Summary of mechanical properties and biological response to the different nanocomposites

Sample	Mechanical properties	Osteoblast proliferation	Mineralisation	Bacterial resistance
PCL/pMWNT	++	0	0	0
PCL/cMWNT	+	+	+	+
PCL/aMWNT	++	+	++	++

where "0" indicates no significant difference, "+" indicates a small but significant improvement, and "++" indicates a much larger significant improvement over PCL.

References

1. A. R. Omran, *The Milbank Memorial Fund Quarterly*, 1971, **49**, 509-538.
2. R. Langer and D. A. Tirrell, *Nature*, 2004, **428**, 487-492.
3. S. L. Ishaug, G. M. Crane, M. J. Miller, A. W. Yasko, M. J. Yaszemski and A. G. Mikos, *Journal of biomedical materials research*, 1997, **36**, 17-28.
4. G. M. Crane, S. L. Ishaug and A. G. Mikos, *Nature Medicine*, 1995, **1**, 1322-1324.
5. L. L. Hench and J. M. Polak, *Science*, 2002, **295**, 1014-1017.
6. M. A. Woodruff and D. W. Hutmacher, *Progress in Polymer Science*, 2010, **35**, 1217-1256.
7. L. Pan, X. Pei, R. He, Q. Wan and J. Wang, *Colloids and Surfaces B: Biointerfaces*, 2012, **93**, 226-234.
8. E. Ural, K. Kesenci, L. Fambri, C. Migliaresi and E. Piskin, *Biomaterials*, 2000, **21**, 2147-2154.
9. C. Wan and B. Chen, *Bimedical Materials*, 2011, **6**, 055010.
10. S. D. McCullen, K. L. Stano, D. R. Stevens, W. A. Roberts, N. A. Monteiro-Riviere, L. I. Clarke and R. E. Gorga, *Journal of Applied Polymer Science*, 2007, **105**, 1668-1678.
11. S. Singh, Y. Pei, R. Miller and P. R. Sundararajan, *Advanced Functional Materials*, 2003, **13**, 868-872.
12. S. Bose, R. A. Khare and P. Moldenaers, *Polymer*, 2010, **51**, 975-993.
13. J. V. Veetil and K. Ye, *Biotechnology progress*, 2009, **25**, 709-721.
14. D. Zhang, M. A. Kandadai, J. Cech, S. Roth and S. A. Curran, *The Journal of Physical Chemistry B*, 2006, **110**, 12910-12915.
15. F. H. Gojny, J. Nastalczyk, Z. Roslaniec and K. Schulte, *Chemical Physics Letters*, 2003, **370**, 820-824.
16. L. Vaisman, H. D. Wagner and G. Marom, *Advances in colloid and interface science*, 2006, **128**, 37-46.
17. R. Shvartzman-Cohen, Y. Levi-Kalisman, E. Nativ-Roth and R. Yerushalmi-Rozen, *Langmuir*, 2004, **20**, 6085-6088.
18. C. Lin, Y. Wang, Y. Lai, W. Yang, F. Jiao, H. Zhang, S. Ye and Q. Zhang, *Colloids and Surfaces B: Biointerfaces*, 2011, **83**, 367-375.
19. M. Bottini, S. Bruckner, K. Nika, N. Bottini, S. Bellucci, A. Magrini, A. Bergamaschi and T. Mustelin, *Toxicology Letters*, 2006, **160**, 121-126.

20. C. M. Sayes, F. Liang, J. L. Hudson, J. Mendez, W. Guo, J. M. Beach, V. C. Moore, C. D. Doyle, J. L. West and W. E. Billups, *Toxicology Letters*, 2006, **161**, 135-142.
21. V. Crescenzi, G. Manzini, G. Calzolari and C. Borri, *European Polymer Journal*, 1972, **8**, 449-463.
22. K. Chatterjee, L. Sun, L. C. Chow, M. F. Young and C. G. Simon Jr, *Biomaterials*, 2011, **32**, 1361-1369.
23. K. Chatterjee, S. Hung, G. Kumar and C. G. Simon, *Journal of Functional Biomaterials*, 2012, **3**, 372-381.
24. V. Krishnan, R. Dhurjati, E. A. Vogler and A. M. Mastro, *In Vitro Cellular & Developmental Biology-Animal*, 2010, **46**, 28-35.
25. Y. Bi, C. H. Stuelten, T. Kilts, S. Wadhwa, R. V. Iozzo, P. G. Robey, X.-D. Chen and M. F. Young, *Journal of Biological Chemistry*, 2005, **280**, 30481-30489.
26. P. Taddei, A. Tinti, M. Reggiani and C. Fagnano, *Journal of Molecular Structure*, 2005, **744–747**, 135-143.
27. E. Weiss, M. Shalhav and Z. Fuss, *Dental Traumatology*, 1996, **12**, 179-184.
28. D. Lahiri, F. Rouzaud, S. Namin, A. Keshri, J. Valdés, L. Kos, N. Tsoukias and A. Agarwal, *ACS applied materials & interfaces*, 2009, **1**, 2470-2476.
29. S. Vardharajula, S. Z. Ali, P. M. Tiwari, E. Eroğlu, K. Vig, V. A. Dennis and S. R. Singh, *International journal of nanomedicine*, 2012, **7**, 5361.
30. J. Cho and D. Paul, *Polymer*, 2001, **42**, 1083-1094.
31. P.-C. Ma, S.-Y. Mo, B.-Z. Tang and J.-K. Kim, *Carbon*, 2010, **48**, 1824-1834.
32. J. Li, Z. Fang, L. Tong, A. Gu and F. Liu, *Journal of Applied Polymer Science*, 2007, **106**, 2898-2906.
33. P.-C. Ma, N. A. Siddiqui, G. Marom and J.-K. Kim, *Composites Part A: Applied Science and Manufacturing*, 2010, **41**, 1345-1367.
34. T. Villmow, B. Kretzschmar and P. Pötschke, *Composites Science and Technology*, 2010, **70**, 2045-2055.
35. Y. Di, S. Iannace, E. Di Maio and L. Nicolais, *Journal of Polymer Science Part B: Polymer Physics*, 2003, **41**, 670-678.
36. T. M. Wu and E. C. Chen, *Journal of Polymer Science Part B: Polymer Physics*, 2006, **44**, 598-606.
37. C. A. Mitchell and R. Krishnamoorti, *Polymer*, 2005, **46**, 8796-8804.
38. K. Wang, W. Li and C. Gao, *Journal of Applied Polymer Science*, 2007, **105**, 629-640.

39. G. Xu, L. Du, H. Wang, R. Xia, X. Meng and Q. Zhu, *Polymer International*, 2008, **57**, 1052-1066.
40. K. Saeed and S. Y. Park, *Journal of Applied Polymer Science*, 2007, **104**, 1957-1963.
41. M. Trujillo, M. L. Arnal, A. J. Müller, M. A. Mujica, C. Urbina de Navarro, B. Ruelle and P. Dubois, *Polymer*, 2012, **53**, 832-841.
42. K. Lu, N. Grossiord, C. E. Koning, H. E. Miltner, B. v. Mele and J. Loos, *Macromolecules*, 2008, **41**, 8081-8085.
43. C. Saujanya and S. Radhakrishnan, *Polymer*, 2001, **42**, 6723-6731.
44. D. Wu, L. Wu, Y. Sun and M. Zhang, *Journal of Polymer Science Part B: Polymer Physics*, 2007, **45**, 3137-3147.
45. M. Ayatollahi, S. Shadlou, M. Shokrieh and M. Chitsazzadeh, *Polymer Testing*, 2011, **30**, 548-556.
46. G. Siqueira, J. Bras and A. Dufresne, *Biomacromolecules*, 2008, **10**, 425-432.
47. S.-Y. Fu, X.-Q. Feng, B. Lauke and Y.-W. Mai, *Composites Part B: Engineering*, 2008, **39**, 933-961.
48. J. N. Coleman, U. Khan, W. J. Blau and Y. K. Gun'ko, *Carbon*, 2006, **44**, 1624-1652.
49. Z. Wang, D. Tang, X. Zheng, W. Zhang and Y. Zhu, *Nanotechnology*, 2007, **18**, 475714.
50. X. Wang, Q. Jiang, W. Xu, W. Cai, Y. Inoue and Y. Zhu, *Carbon*, 2012.
51. S. Nuriel, L. Liu, A. Barber and H. Wagner, *Chemical physics letters*, 2005, **404**, 263-266.
52. R. Flemming, C. Murphy, G. Abrams, S. Goodman and P. Nealey, *Biomaterials*, 1999, **20**, 573-588.
53. N. R. Washburn, K. M. Yamada, C. G. Simon Jr, S. B. Kennedy and E. J. Amis, *Biomaterials*, 2004, **25**, 1215-1224.
54. Y. Qi, Z. Tai, D. Sun, J. Chen, H. Ma, X. Yan, B. Liu and Q. Xue, *Journal of Applied Polymer Science*, 2013, **127**, 1885-1894.
55. M. A. Correa-Duarte, N. Wagner, J. Rojas-Chapana, C. Morsczeck, M. Thie and M. Giersig, *Nano Letters*, 2004, **4**, 2233-2236.
56. J. R. Venugopal, S. Low, A. T. Choon, A. B. Kumar and S. Ramakrishna, *Artificial organs*, 2008, **32**, 388-397.
57. D. W. Hutmacher, T. Schantz, I. Zein, K. W. Ng, S. H. Teoh and K. C. Tan, *Journal of biomedical materials research*, 2001, **55**, 203-216.
58. P. E. Mikael and S. P. Nukavarapu, *Journal of Biomaterials and Tissue Engineering*, 2011, **1**, 76-85.

59. X. Li, H. Gao, M. Uo, Y. Sato, T. Akasaka, Q. Feng, F. Cui, X. Liu and F. Watari, *Journal of Biomedical Materials Research Part A*, 2009, **91**, 132-139.
60. K.-W. Lee, S. Wang, M. J. Yaszemski and L. Lu, *Biomaterials*, 2008, **29**, 2839-2848.
61. J. Wei, T. Igarashi, N. Okumori, T. Igarashi, T. Maetani, B. Liu and M. Yoshinari, *Biomedical Materials*, 2009, **4**, 045002.
62. H. Nikukar, S. Reid, M. P. Tsimbouri, M. O. Riehle, A. S. Curtis and M. J. Dalby, *ACS nano*, 2013.
63. B. M. Spiegelman and C. A. Ginty, *Cell*, 1983, **35**, 657-666.
64. R. McBeath, D. M. Pirone, C. M. Nelson, K. Bhadriraju and C. S. Chen, *Developmental cell*, 2004, **6**, 483-495.
65. G. Kumar, C. K. Tison, K. Chatterjee, P. S. Pine, J. H. McDaniel, M. L. Salit, M. F. Young and C. G. Simon Jr, *Biomaterials*, 2011, **32**, 9188-9196.
66. B. G. Keselowsky, D. M. Collard and A. J. García, *Proceedings of the National Academy of Sciences*, 2005, **102**, 5953-5957.
67. M. Celeste R áTria and R. A. May V áVergara, *Chemical Communications*, 2011, **47**, 8892-8894.
68. S. Liu, T. H. Zeng, M. Hofmann, E. Burcombe, J. Wei, R. Jiang, J. Kong and Y. Chen, *ACS nano*, 2011, **5**, 6971-6980.
69. S. Kang, M. Herzberg, D. F. Rodrigues and M. Elimelech, *Langmuir*, 2008, **24**, 6409-6413.
70. V. K. Upadhyayula, S. Deng, M. C. Mitchell and G. B. Smith, *Science of the total environment*, 2009, **408**, 1-13.
71. I. E. M. Carpio, C. M. Santos, X. Wei and D. F. Rodrigues, *Nanoscale*, 2012, **4**, 4746-4756.
72. O. Akhavan and E. Ghaderi, *ACS nano*, 2010, **4**, 5731-5736.
73. S. Kang, M. Pinault, L. D. Pfefferle and M. Elimelech, *Langmuir*, 2007, **23**, 8670-8673.
74. A. Isquith, E. Abbott and P. Walters, *Applied Microbiology*, 1972, **24**, 859-863.
75. E. F. Palermo, D.-K. Lee, A. Ramamoorthy and K. Kuroda, *The Journal of Physical Chemistry B*, 2010, **115**, 366-375.

Figure captions:

Figure 1: SEM micrographs of the cross sectional cryofractured surface of: scale bar = 5 μm and inserts scale bar of = 1 μm

Figure 2: DSC scans of (a) melting endotherm and (b) crystallization exotherm of PCL, PCL/pMWNT, PCL/cMWNT and PCL/aMWNT nanocomposites

Figure 3 X-ray diffraction spectra of neat PCL, PCL/pMWNT, PCL/cMWNT and PCL/aMWNT nanocomposites

Figure 4 Rheological data for PCL, PCL/pMWNT, PCL/aMWNT and PCL/cMWNT nanocomposites: (a) storage modulus and (b) complex viscosity as a function of frequency

Figure 5: Mechanical properties of PCL and its nanocomposites: (a) representative stress-strain curves, (b) elastic modulus and (c) tensile strength. Results are represented as mean ± SD for n = 5. Statistically significant difference ($p < 0.05$) compared to neat PCL and PCL/cMWNT are indicated by * and ♦, respectively.

Figure 6: Water contact angle of PCL, PCL/pMWNT, PCL/cMWNT and PCL/aMWNT nanocomposites surfaces. Results are represented as mean ± SD for n = 3. Statistically significant difference ($p < 0.05$) compared to neat PCL and PCL/pMWNT are indicated by * and ♦ respectively

Figure 7: Surface height topography obtained from AFM micrographs for sample: (a) PCL, (b) PCL/pMWNT, (c) PCL/cMWNT, and (d) PCL/aMWNT

Figure 8: DNA quantification for osteoblasts cultured on the PCL and its nanocomposite surfaces at 1d, 6d, and 10d. Results are expressed as mean ± SD for n = 14. Statistically

significant differences ($p < 0.05$) compared to neat PCL and PCL/pMWNT at a given day are indicated by the symbols ∗ and ♦, respectively.

Figure 9: Fluorescent micrographs of cell nuclei on PCL, PCL/aMWNT, PCL/cMWNT and PCL/pMWNT nanocomposite substrates (scale bar = 0.5 mm)

Figure 10: Osteoblast morphology on PCL, PCL/pMWNT, PCL/cMWNT and PCL/aMWNT nanocomposites (scale bar = 50 μm); (a) Aspect ratio and (b) Surface area. Statistically significant differences ($p < 0.05$) compared to neat PCL and PCL/pMWNT are indicated by the symbols ∗ and ♦, respectively

Figure 11: (a) FTIR spectra of neat PCL and Mineralized PCL/aMWNT disc, (b) Quantification of calcium deposition by Alizarin Red S staining on PCL and the nanocomposites. Statistically significant differences ($p < 0.05$) compared to neat PCL, PCL/pMWNT and PCL/cMWNT at a given day are indicated by the symbols ∗, ♦ and ⊗, respectively

Figure 12: OD measurements for bacterial growth for neat PCL, PCL/aMWNT, PCL/cMWNT, PCL/pMWNT nanocomposites and control. Statistically significant differences ($p < 0.05$) compared to neat PCL, PCL/pMWNT and PCL/cMWNT shown for 12 h culture and are indicated by the symbols ∗, ♦ and ⊗, respectively

Figure 13: SEM micrograph of *Escherichia coli* adhesion to PCL, PCL/aMWNT, PCL/cMWNT and PCL/pMWNT nanocomposites surfaces after 8 h culture; scale bar = 30 μm

Figures

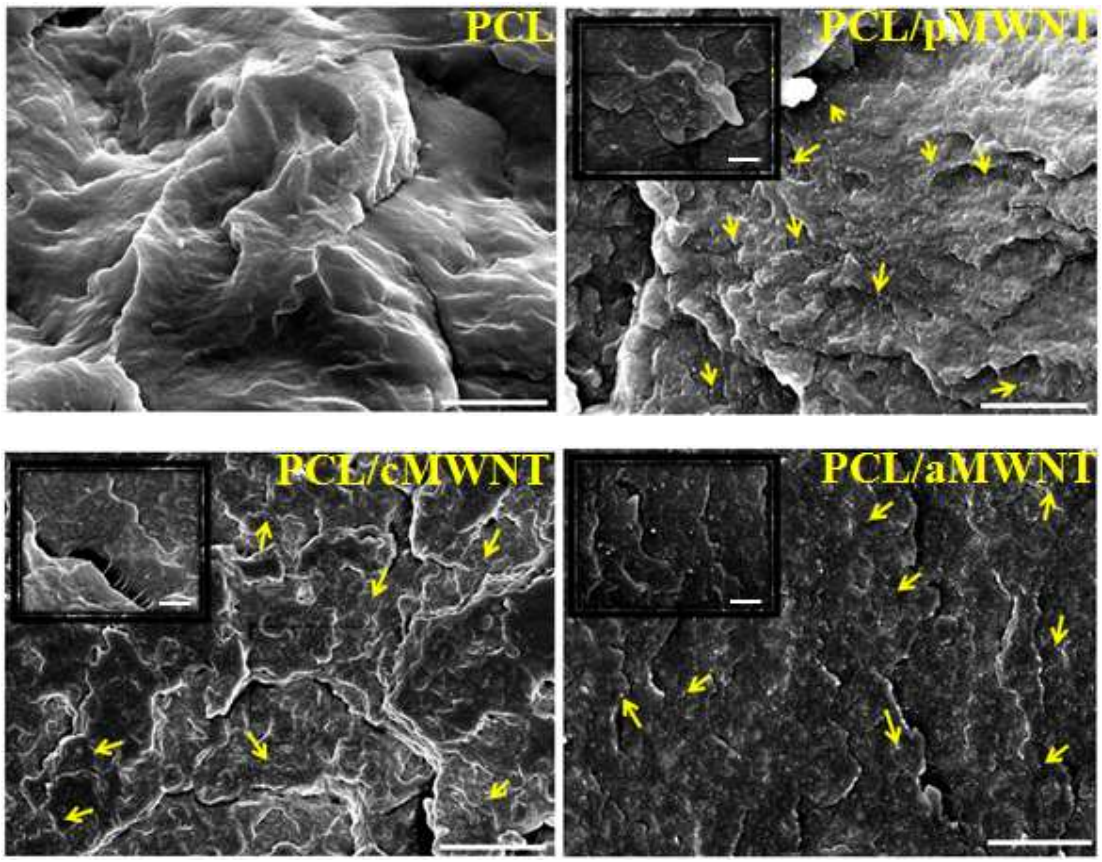

Figure 1: SEM micrographs of the cross sectional cryofractured surface of: scale bar = 5 μm and inserts scale bar of = 1 μm

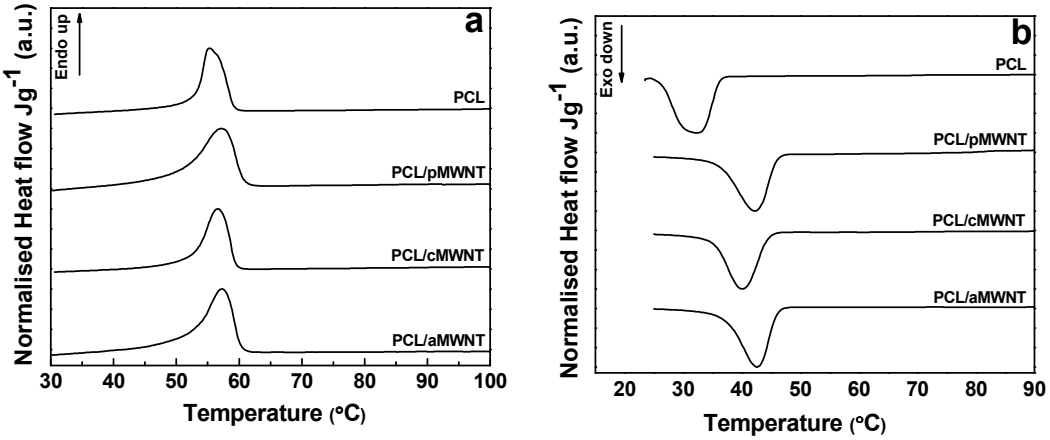

Figure 2: DSC scans of (a) melting endotherm and (b) crystallization exotherm of PCL, PCL/pMWNT, PCL/cMWNT and PCL/aMWNT nanocomposites

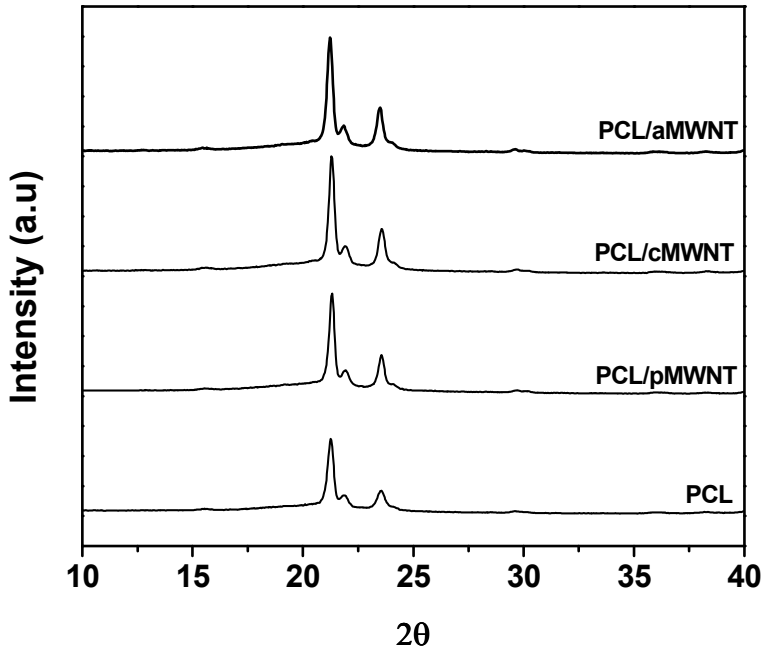

Figure 3 X-ray diffraction spectra of neat PCL, PCL/pMWNT, PCL/cMWNT and PCL/aMWNT nanocomposites

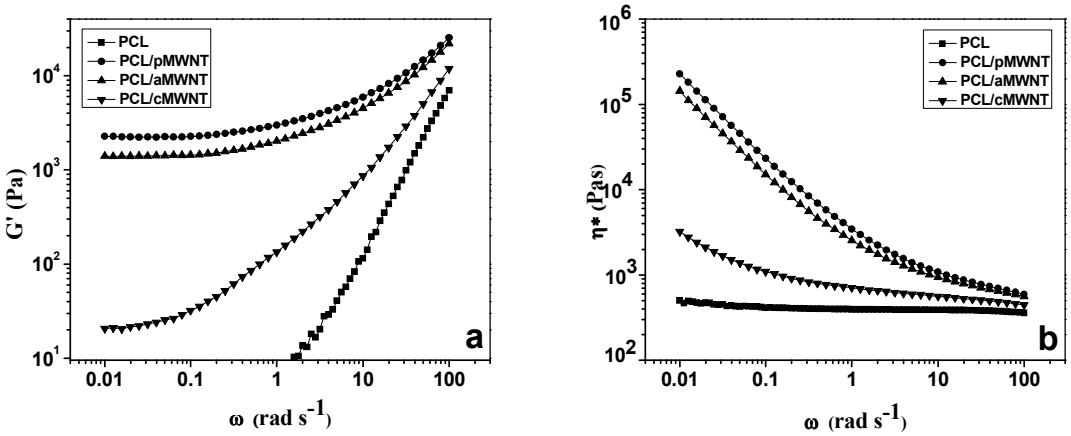

Figure 4 Rheological data for PCL, PCL/pMWNT, PCL/aMWNT and PCL/cMWNT nanocomposites: (a) storage modulus and (b) complex viscosity as a function of frequency

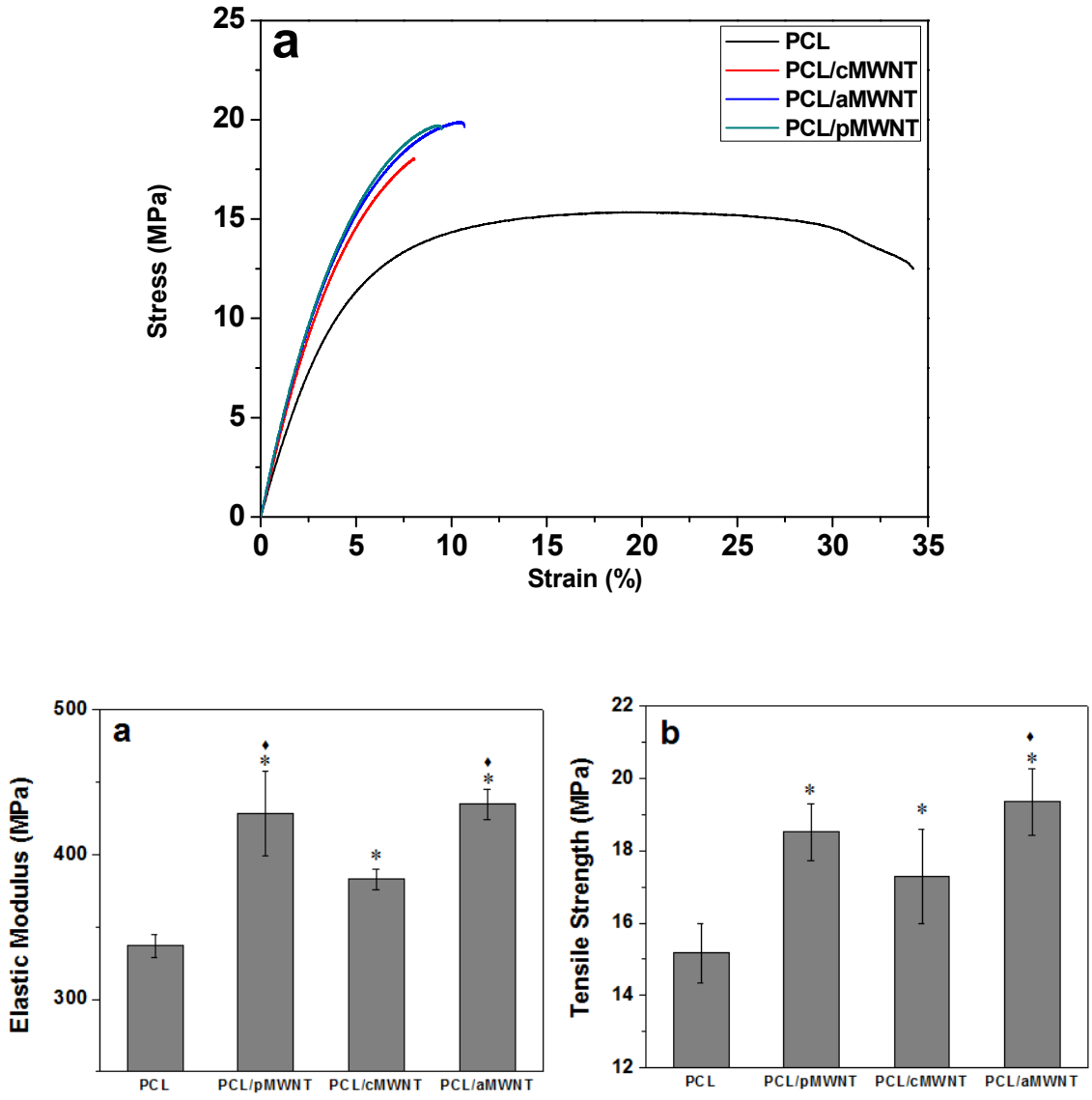

Figure 5: Mechanical properties of PCL and its nanocomposites: (a) representative stress-strain curves, (b) elastic modulus and (c) tensile strength. Results are represented as mean ± SD for n = 5. Statistically significant difference ($p < 0.05$) compared to neat PCL and PCL/cMWNT are indicated by * and ♦, respectively.

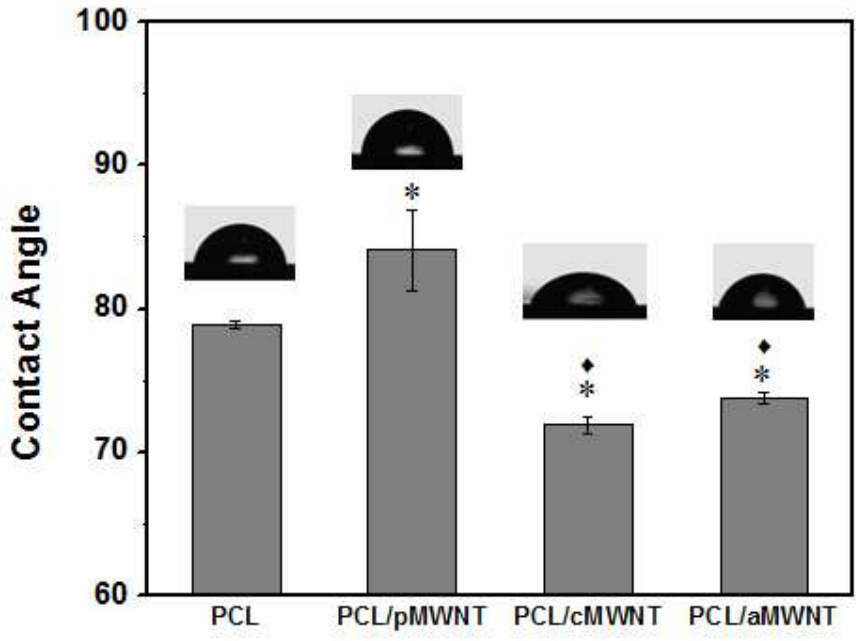

Figure 6: Water contact angle of PCL, PCL/pMWNT, PCL/cMWNT and PCL/aMWNT nanocomposites surfaces. Results are represented as mean ± SD for n = 3. Statistically significant difference ($p < 0.05$) compared to neat PCL and PCL/pMWNT are indicated by * and ♦ respectively

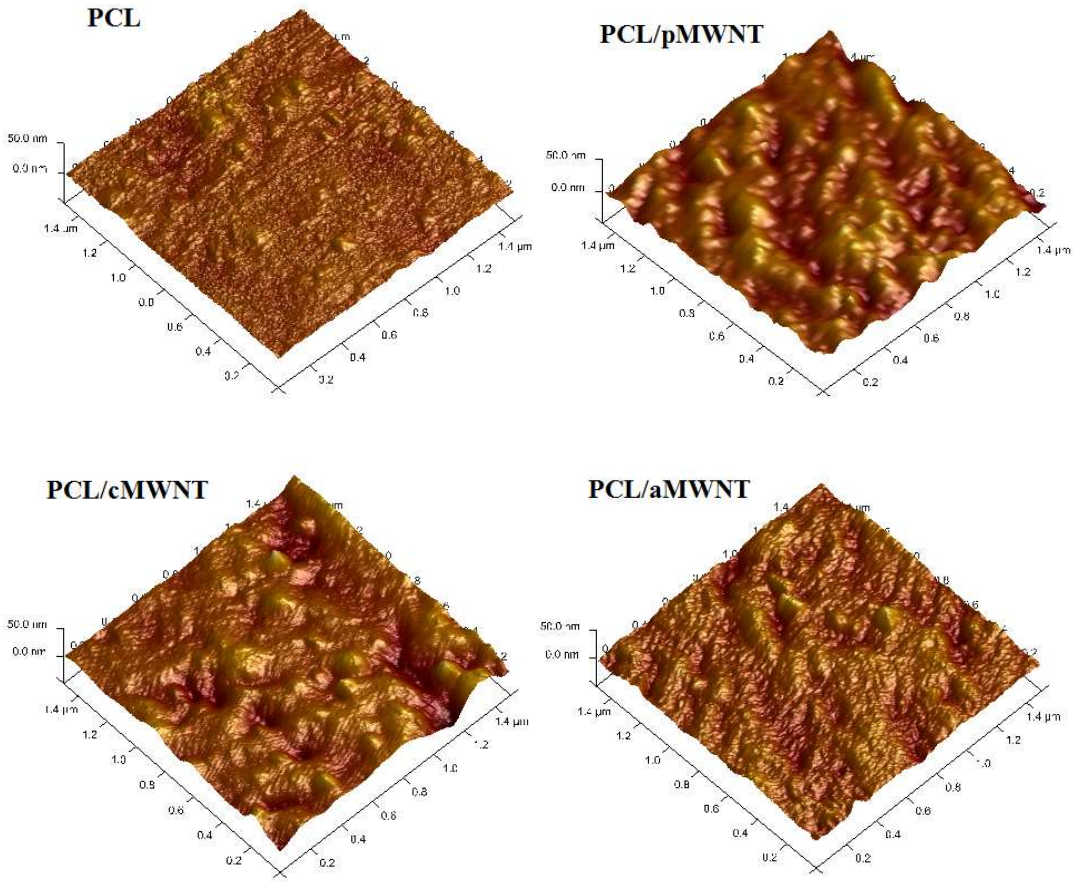

Figure 7: Surface height topography obtained from AFM micrographs for sample: (a) PCL, (b) PCL/pMWNT, (c) PCL/cMWNT, and (d) PCL/aMWNT

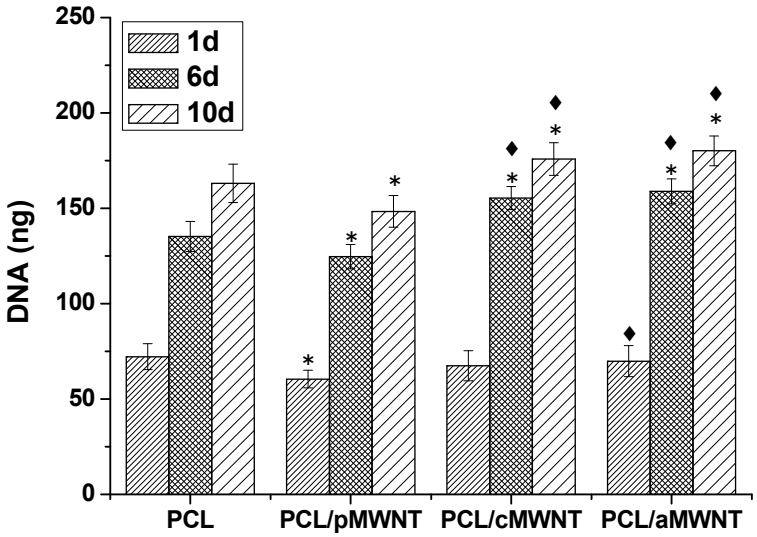

Figure 8: DNA quantification for osteoblasts cultured on the PCL and its nanocomposite surfaces at 1d, 6d, and 10d. Results are expressed as mean ± SD for n = 14. Statistically significant differences ($p < 0.05$) compared to neat PCL and PCL/pMWNT at a given day are indicated by the symbols ∗ and ♦, respectively.

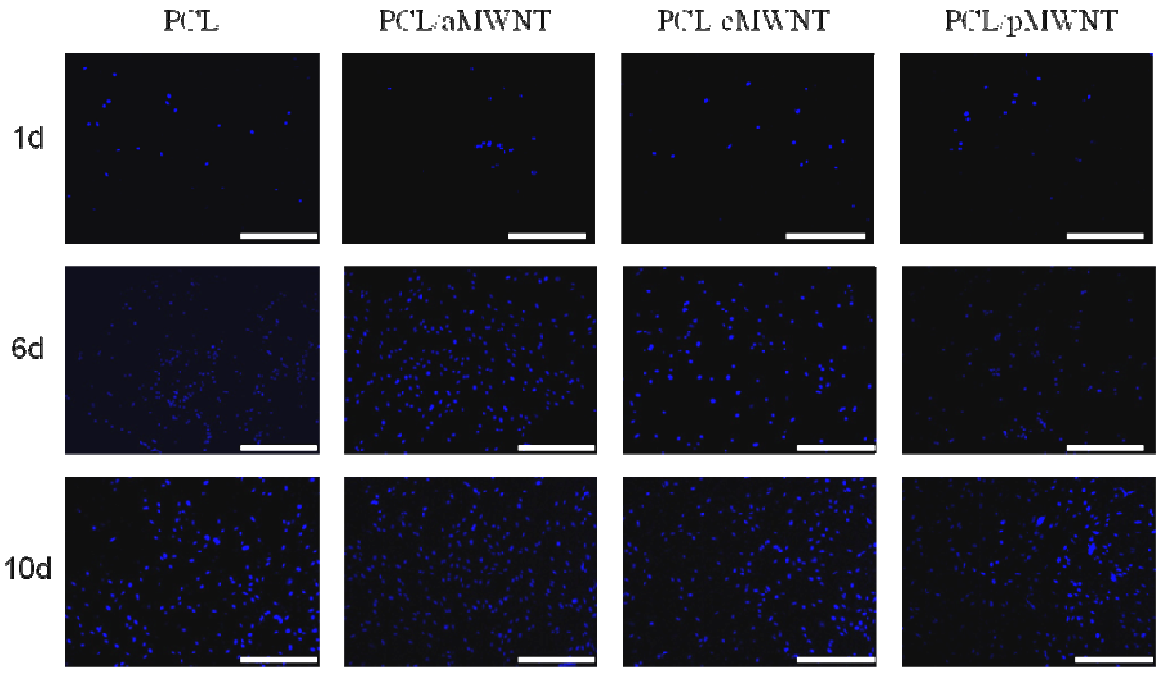

Figure 9: Fluorescent micrographs of cell nuclei on PCL, PCL/aMWNT, PCL/cMWNT and PCL/pMWNT nanocomposite substrates (scale bar = 0.5 mm)

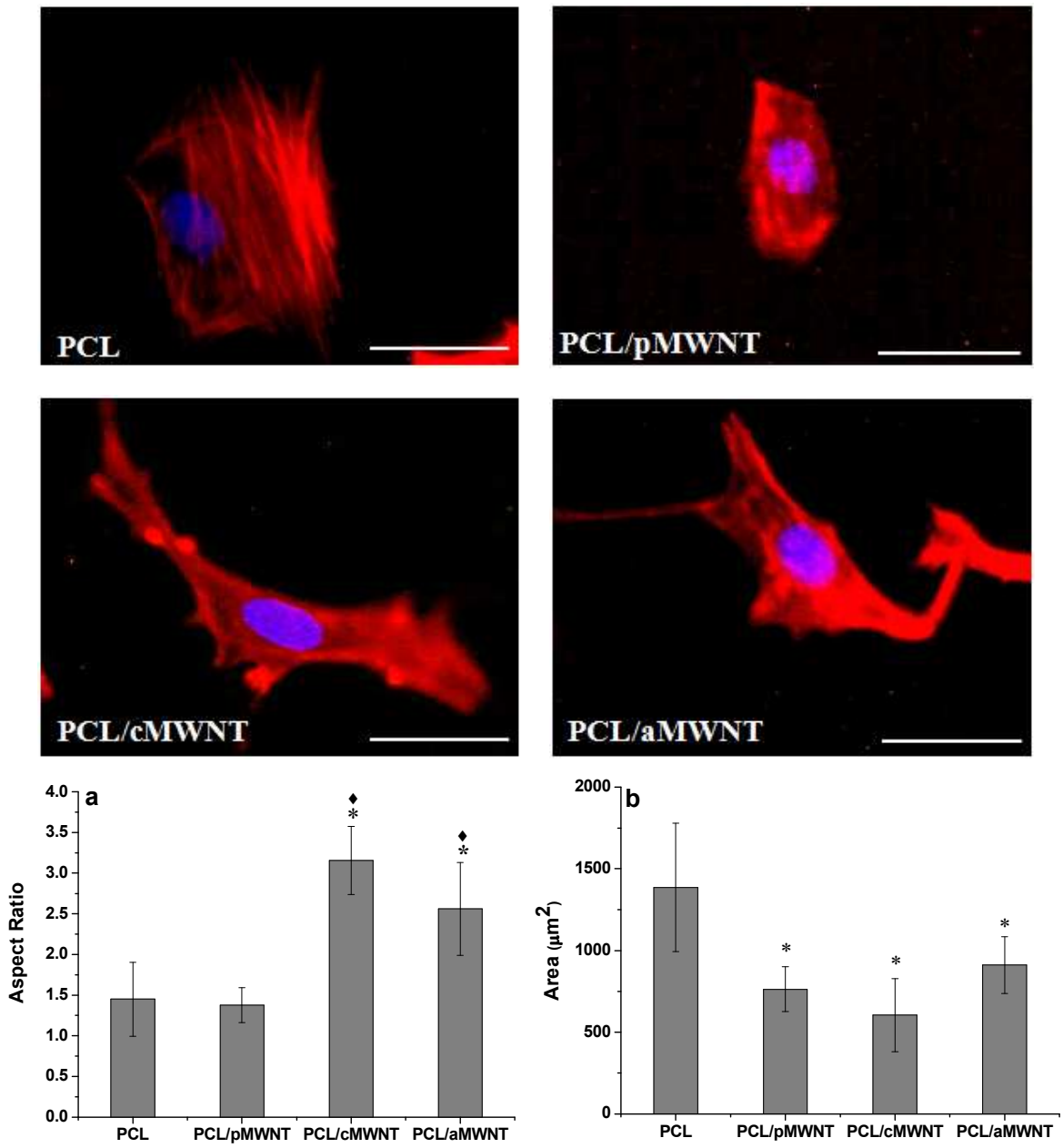

Figure 10: Osteoblast morphology on PCL, PCL/pMWNT, PCL/cMWNT and PCL/aMWNT nanocomposites (scale bar = 50 μm); (a) Aspect ratio and (b) Surface area. Statistically significant differences ($p < 0.05$) compared to neat PCL and PCL/pMWNT are indicated by the symbols ∗ and ♦, respectively

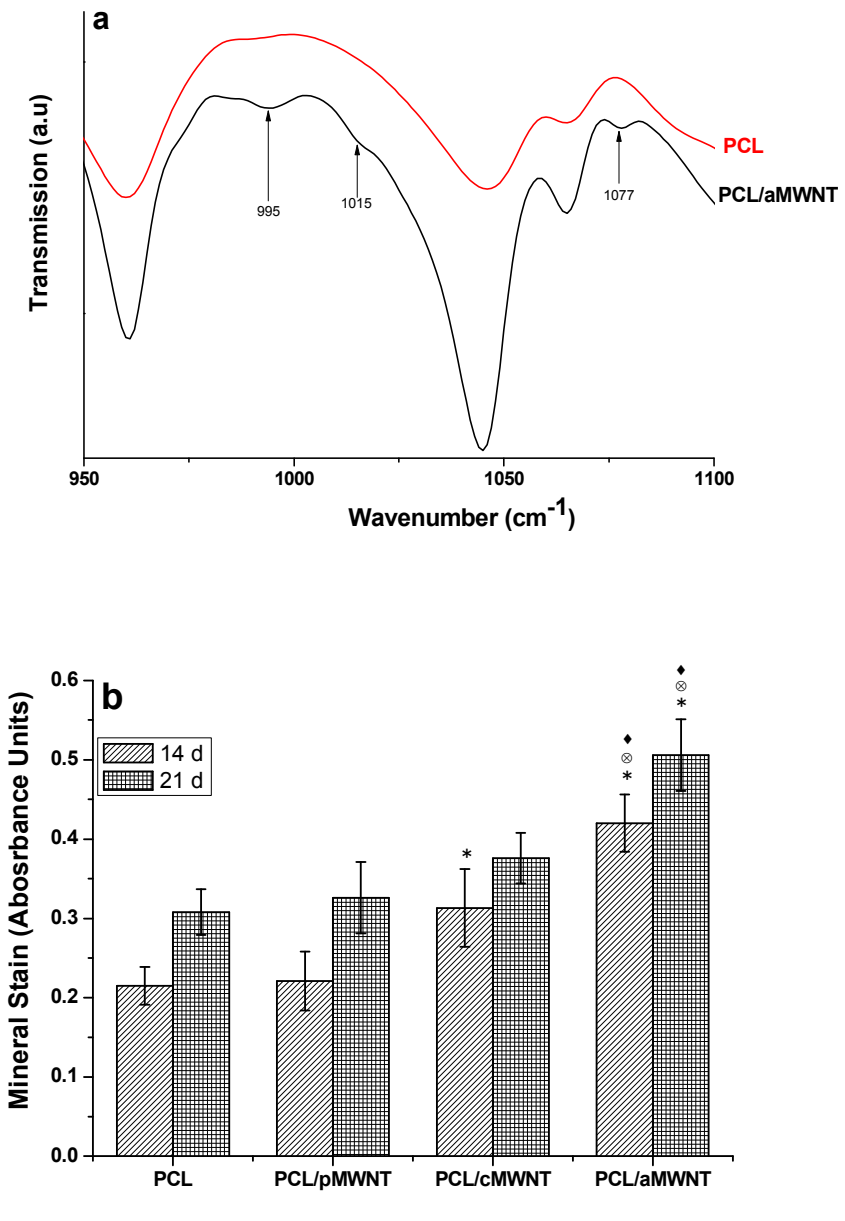

Figure 11: (a) FTIR spectra of neat PCL and Mineralized PCL/aMWNT disc, (b) Quantification of calcium deposition by Alizarin Red S staining on PCL and the nanocomposites. Statistically significant differences ($p < 0.05$) compared to neat PCL, PCL/pMWNT and PCL/cMWNT at a given day are indicated by the symbols ∗, ♦ and ⊗, respectively

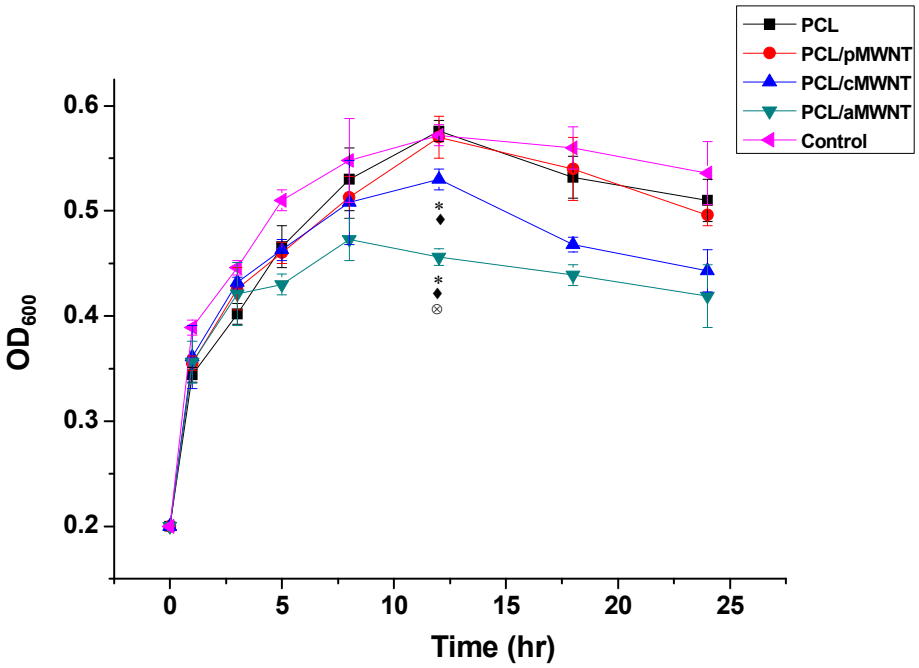

Figure 12: OD measurements for bacterial growth for neat PCL, PCL/aMWNT, PCL/cMWNT, PCL/pMWNT nanocomposites and control. Statistically significant differences ($p < 0.05$) compared to neat PCL, PCL/pMWNT and PCL/cMWNT shown for 12 h culture and are indicated by the symbols ∗, ♦ and ⊗, respectively

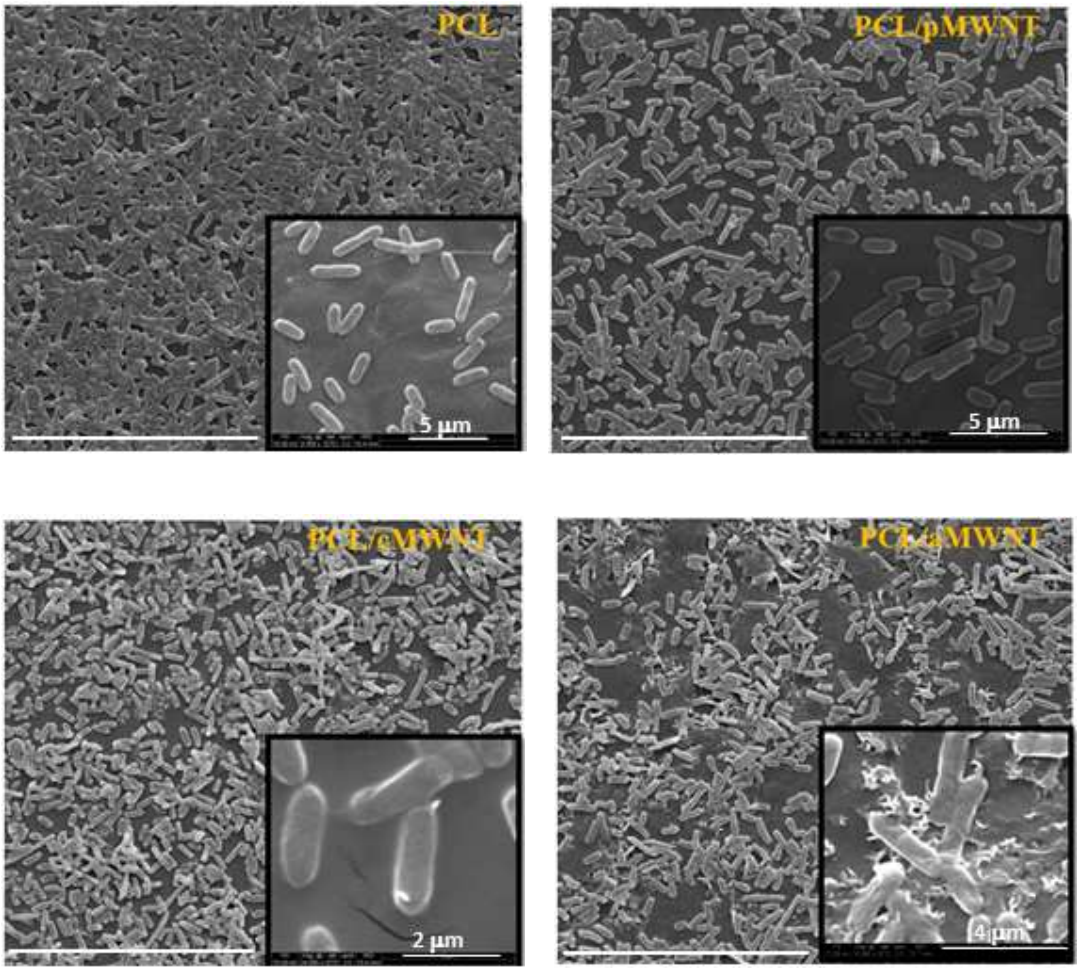

Figure 13: SEM micrograph of *Escherichia coli* adhesion to PCL, PCL/aMWNT, PCL/cMWNT and PCL/pMWNT nanocomposites surfaces after 8 h culture; scale bar = 30 µm